

# Robust Dynamic State Estimation for Power System Based on Adaptive Cubature Kalman Filter with Generalized Correntropy Loss

Yaoqiang Wang, *Senior Member, IEEE*, Zhiwei Yang, *Student Member, IEEE*, Yi Wang, *Member, IEEE*, Venkata Dinavahi, *Fellow, IEEE*, Jun Liang, *Senior Member, IEEE*, and Kewen Wang, *Member, IEEE*

**Abstract**—Due to the unfavorable interference of non-Gaussian noise, abnormal system states, and rough measurement errors, dynamic state estimation (DSE) plays an important role in the safe operation of power system. A novel DSE method based on an adaptive cubature Kalman filter (CKF) with generalized correntropy loss (GCL) criterion, termed AGCLCKF, is developed to deal with the complex non-Gaussian distribution noises of power system in this paper. First, a nonlinear regression model is derived to simultaneously incorporate the state and noise errors into the GCL cost function, and a fixed-point iteration is exploited to recursively update the posterior state estimate. Then, considering that the filtering performance of the estimator is largely determined by the kernel bandwidth in correntropy, an adaptive factor is established to adjust the kernel bandwidth of kernel function in real-time, which can improve the flexibility and accuracy of dynamic state estimation in the existence of bad measurement information. Finally, extensive simulation results carried out on the IEEE 39-bus test system demonstrate that the proposed method can achieve much accuracy and robustness under various situations.

**Index Terms**—Adaptive factor, cubature Kalman filter (CKF), generalized correntropy loss (GCL), non-Gaussian noise, power system dynamic state estimator, synchronous generator modeling.

## I. INTRODUCTION

Accurate and reliable state estimation (SE) plays an important role in the domain of power system, such as line protection, parameter identification, emergency control etc. [1]-[5]. In previous studies, the transmission and

This work was supported in part by the National Natural Science Foundation of China under Grant 51507155, in part by the Youth Key Teacher Project of Henan Universities under Grant 2019GGJS011, in part by the Scientific and Technological Research Project of Henan Province under Grant 222102520001, and in part by Henan Postdoctoral Foundation. (Corresponding author: Yi Wang.)

Yaoqiang Wang, Zhiwei Yang, Yi Wang, and Kewen Wang are with the School of Electrical Engineering, Zhengzhou University, Zhengzhou 450001, China, and also with the Henan Engineering Research Center of Power Electronics and Energy Systems, Zhengzhou 450001, China (e-mails: WangyqEE@163.com; 13253319984@163.com; wangyi1414599008@163.com; kwwang@zzu.edu.cn).

Jun Liang is with the School of Electrical Engineering, Zhengzhou University, Zhengzhou 450001, China, and also with the School of Engineering, Cardiff University, Cardiff CF24 3AA, UK (e-mail: liangjl@cardiff.ac.uk).

Venkata Dinavahi is with the Department of Electrical and Computer Engineering, University of Alberta, Edmonton, AB T6G 1H9, Canada (e-mail: dinavahi@ualberta.ca).

distribution networks are usually regarded as the research focus of static state estimation since it is the basis for the stable operation of the power grid [6]. As one of the key factors affecting the normal operation of power system, the state estimation of synchronous generator is also paramount [7]. Dynamic state estimation (DSE), through real-time monitoring and tracking with phasor measurement unit (PMU), can provide an optimal solution for the dynamic change of generator states.

In recent years, Kalman filter (KF), a recursive least squares linear filter [8] and its non-linear extension variants, such as extended Kalman filter (EKF) [9], unscented Kalman filter (UKF) [10], [11], and cubature Kalman filter (CKF) [12], [13] have been widely utilized in the dynamic state estimation. Considering the unknown noise statistics and the uncertainty of the model parameters, by incorporating the robust control theory with the traditional EKF approach, a robust HEKF filter was proposed to estimate the states of power system [14]. An improved EKF with multi-step adaptive interpolation technique was established to achieve a balance between computational efficiency and estimation accuracy [15]. In order to mitigate the approximation error caused by the linearization procedure of EKF, several derivative-free filters were further developed [16]-[18]. A robust UKF approach with positive semidefinite estimation error covariance was proposed to enhance the numerical stability of the filter [16]. The decentralized derivative free UKF-based DSE with several unknown inputs was advocated to estimate the state variables of generator [17]. To deal with the adverse effects of the bimodal Gaussian mixture measurement errors, a hybrid robust estimator combining generalized maximum-likelihood and CKF (GM-CKF) was proposed [18]. It is worth pointing out that the cost function of the above KF-based system model obeys the minimum mean square error (MSE) loss criterion, which follows the Gaussian noise distribution and means that these methods are easily sensitive to the non-Gaussian noise, such as heavy tailed types [19], [20]. Therefore, the performance of these methods can degrade seriously in the presence of the non-Gaussian noise conditions.

In order to deal with the above issues, some robust dynamic state estimation methods for power system dynamic state estimation were developed. In [21] and [22], the H-infinity methodology was utilized to enhance the robustness against model uncertainties. The Huber estimator and M-estimation

theory were developed to mitigate the adverse effects of observation outliers [18], [23]. In addition, motivated by the information theoretic learning, the concept of correntropy based on the Gaussian kernel has been vigorously developed and widely used in machine learning and automatic control recently [24]-[26], which can effectively capture the higher-order error statistics, especially for the non-Gaussian noise error [27], [28]. However, the Gaussian kernel is likely to fail in actual power system due to the singularity of specific type of noise with Gaussian function. To address this problem, the generalized correntropy was developed in [29]. Compared with the correntropy based on the Gaussian kernel, the shape of correntropy can be freely transformed by utilizing the generalized Gaussian density function. Meanwhile, the research on generalized correntropy loss is further compared and analyzed in [30]. In addition, it is worth noting that the influence of the kernel parameters on the estimated results needs to be further investigated according to [31]-[34]. In fact, an unsuitable kernel parameter of correntropy can affect the performance of state estimation greatly. Specifically, a too large kernel bandwidth (KB) can severely limit the ability of filter to suppress outliers, while a too small KB may lead to slow convergence and even divergence of filtering. So far, there is still no method to effectively adjust the kernel bandwidth in generalized correntropy.

In view of the aforementioned researches, in order to further solve the complex non-Gaussian noise interference in power system, a novel robust DSE methodology based on adaptive cubature Kalman filter with generalized correntropy loss strategy (termed as AGCLCKF) is developed in this paper. The main contributions of this paper are threefold.

- By utilizing the GCL optimal criterion and the nonlinear regression model to adjust the state and noise covariance matrices, the proposed method with a suitable kernel bandwidth can achieve strong robustness against the non-Gaussian noise.
- The utilization of the adaptive factor  $\mu_k$  can dynamically update the kernel bandwidth according to the changes of measurements, which can further improve the flexibility of the algorithm and the robust performance in the presence of abnormal measurement.
- Extensive comparative studies under various operating conditions have been carried out to validate that AGCLCKF can achieve much better performance in terms of estimation accuracy and robustness under the non-Gaussian noise conditions.

The remainder of this paper is organized as follows. The dynamic state estimation model of power system is established and analyzed in Section II. The GCL algorithm based on CKF and the adaptive strategy of kernel bandwidth are developed and introduced detailed in Section III. Extensive numerical simulations carried out on the IEEE 39-bus test system under various circumstances are provided to demonstrate the efficacy of the proposed method in Section IV. Finally, conclusions are drawn in Section V.

## II. DYNAMIC STATE ESTIMATION MODEL OF POWER SYSTEM

Compared with the classical second-order generator model [22], this paper considers the electromagnetic dynamic process of generator  $d$ ,  $q$ ,  $f$ ,  $g$ ,  $D$  and  $Q$  windings, while the dynamic process of  $D$ ,  $Q$  windings and stator in the sub transient process are ignored. Then, a more accurate and simplified nonlinear fourth-order generator model can be obtained [21]. The detailed generator state model can be described by

$$\dot{\delta} = \omega - \omega_0, \quad (1)$$

$$\dot{\omega} = \frac{\omega_0}{2T_j} \left[ T_m - T_e - \frac{K_D}{\omega_0} (\omega - \omega_0) \right], \quad (2)$$

$$\dot{e}'_q = \frac{1}{T'_{d0}} \left[ E'_{fd} - e'_q - (x_d - x'_d) i_d \right], \quad (3)$$

$$\dot{e}'_d = \frac{1}{T'_{q0}} \left[ -e'_d + (x_q - x'_q) i_q \right], \quad (4)$$

where  $\delta$  indicates the absolute power angle of generator rotor;  $\omega$  and  $\omega_0$  are the electrical angular velocity and its initial value, respectively;  $T_j$  denotes the inertia constant,  $K_D$  indicates the damping coefficient;  $T_m$  and  $T_e$  represent the mechanical and electromagnetic power of the generator, respectively;  $e'_q$  and  $e'_d$  represent the  $q$ -axis and  $d$ -axis transient electromotive force of generator, respectively;  $E'_{fd}$  is the excitation voltage of generator stator;  $x_d$  and  $x'_d$  are synchronous reactance and transient reactance of generator  $d$ -axis, respectively;  $T'_{d0}$  and  $T'_{q0}$  are the open-circuit transient time constants of generator  $q$ -axis and  $d$ -axis, respectively;  $i_d$  and  $i_q$  represent the stator currents on the  $d$ -axis and  $q$ -axis of generator, respectively;  $x_q$  and  $x'_q$  respectively denote the synchronous reactance and transient reactance on  $q$ -axis.

For the DSE of power system, a time-varying and discrete characteristics physical model consisting of state and measurement variables must be established in advance. By utilizing the improved Euler approach [21], the discrete-time nonlinear model for the generator can be expressed as

$$\begin{cases} \mathbf{x}_k = \boldsymbol{\phi}(\mathbf{x}_{k-1}, \mathbf{u}_{k-1}) + \mathbf{w}_{k-1} \\ \mathbf{z}_k = \mathbf{h}(\mathbf{x}_k, \mathbf{u}_k) + \mathbf{v}_k \end{cases}, \quad (5)$$

$$\mathbf{x}_k = [\delta \ \omega \ e'_q \ e'_d]^T, \quad (6.a)$$

$$\mathbf{u}_k = [T_m \ E_{fd} \ i_R \ i_I]^T, \quad (6.b)$$

$$\mathbf{z}_k = [\delta \ \omega \ e_R \ e_I]^T, \quad (6.c)$$

where  $\boldsymbol{\phi}(\cdot)$  and  $\mathbf{h}(\cdot)$  are the state propagation function and vector-valued output function, respectively;  $\mathbf{x} \in \mathbf{R}^n$  represents the state vector composed of rotor power angle  $\delta$ , angular velocity  $\omega$ , transient electromotive force on the  $q$ -axis  $e'_q$  and  $d$ -axis  $e'_d$  of generator; the measurement vector  $\mathbf{z} \in \mathbf{R}^m$  consists of power angle  $\delta$ , angular velocity  $\omega$  and stator voltage on  $R$ -axis  $e_R$  and  $I$ -axis  $e_I$ ;  $\mathbf{u}$  comprises of generator mechanical power  $T_m$ , stator excitation voltage  $E_{fd}$  and stator

$R$ -axis and  $I$ -axis currents  $i_R$  and  $i_I$ ;  $\mathbf{w}_k$  and  $\mathbf{v}_k$  respectively indicate the system noise and measurement device noise, which are usually assumed as the Gaussian white noise with mean value of zero and covariance of  $\mathbf{Q}_k$  and  $\mathbf{R}_k$ , respectively; the subscript  $k$  represents the time instant.

By rewriting the  $e_R$ ,  $e_I$ ,  $i_d$ , and  $i_q$  as functions of  $\mathbf{x}_k$  and  $\mathbf{u}_k$ , the state propagation function and measurement functions can be implemented as general state space model (5)

$$e_R = (e'_d + i_d x'_q) \sin(\delta) + (e'_q - i_d x'_d) \cos(\delta), \quad (7)$$

$$e_I = (e'_q - i_d x'_d) \sin(\delta) - (e'_d + i_q x'_q) \cos(\delta), \quad (8)$$

$$i_d = i_R \sin(\delta) - i_I \cos(\delta), \quad (9)$$

$$i_q = i_I \sin(\delta) + i_R \cos(\delta). \quad (10)$$

### III. ADAPTIVE GENERALIZED CORRENTROPY LOSS CUBATURE KALMAN FILTER WITH NONLINEAR REGRESSION

In this section, based on the GCL criteria and CKF framework, by combining the noise statistics with the kernel width adaptive update strategy, a novel AGCLCKF algorithm against the non-Gaussian noise is designed and introduced in detail.

#### A. Generalized Correntropy Loss Criterion

Inspired by the information theoretic learning, supposing two random variables  $\mathbf{X}$  and  $\mathbf{Y}$ , the correntropy is formally defined as [29]

$$V(\mathbf{X}, \mathbf{Y}) = E[\kappa_\sigma(\mathbf{X}, \mathbf{Y})] = \int \kappa_\sigma(\mathbf{x}, \mathbf{y}) dF_{\mathbf{X}, \mathbf{Y}}(\mathbf{x}, \mathbf{y}), \quad (11)$$

where  $E(\cdot)$  stands for the expectation operator,  $F_{\mathbf{X}, \mathbf{Y}}(\mathbf{x}, \mathbf{y})$  denotes the joint probability distribution of  $(\mathbf{X}, \mathbf{Y})$ ;  $\kappa_\sigma(\cdot)$  represents the shift-invariant Mercer kernel with kernel bandwidth  $\sigma$ , where the Gaussian kernel is generally the most commonly used.

Based on (11), in order to deal with the non-Gaussian noise effectively, a more flexible generalized Gaussian density kernel with zero mean is developed, which can be expressed by

$$\begin{aligned} G_{\alpha, \beta}(\mathbf{X}, \mathbf{Y}) &= \frac{\alpha}{2\beta \Gamma\left(\frac{1}{\alpha}\right)} \exp\left\{-\left|\frac{\mathbf{X} - \mathbf{Y}}{\beta}\right|^\alpha\right\} \\ &= \xi_{\alpha, \beta} \exp\{-\varphi |\mathbf{X} - \mathbf{Y}|^\alpha\}, \end{aligned} \quad (12)$$

where  $\Gamma(\cdot)$  is the gamma function,  $\xi_{\alpha, \beta} = \alpha / (2\beta \Gamma(1/\alpha))$  represents the normalization coefficient;  $\alpha$  and  $\beta$  represent the shape parameter and the width of kernel, respectively;  $\varphi = 1/\beta^\alpha$  is related to kernel parameters; Note that if  $\alpha = 2$  and  $\beta = \sqrt{2}\sigma$  ( $\sigma$  is the kernel bandwidth of correntropy), GCL degenerates into the maximum correntropy criterion (MCC).

Therefore, (11) can be further defined as follows

$$V_{\alpha, \beta}(\mathbf{X}, \mathbf{Y}) = \mathbb{E}[G_{\alpha, \beta}(\mathbf{X}, \mathbf{Y})]. \quad (13)$$

Due to the unknowability of the joint probability density and the finite number of samples  $\{\mathbf{x}_i, \mathbf{y}_i\}_{i=1}^N$  in actual situations,

the estimator of the GCL between  $\mathbf{X}$  and  $\mathbf{Y}$  is further expressed as

$$\hat{V}_{\alpha, \beta}(\mathbf{X}, \mathbf{Y}) = \frac{1}{N} \sum_{i=1}^N G_{\alpha, \beta}(\mathbf{x}_i, \mathbf{y}_i), \quad (14)$$

$$\begin{aligned} \hat{J}_{GCL}(\mathbf{X}, \mathbf{Y}) &= G_{\alpha, \beta}(0, 0) - \hat{V}_{\alpha, \beta}(\mathbf{X}, \mathbf{Y}) \\ &= \xi_{\alpha, \beta} - \frac{1}{N} \sum_{i=1}^N G_{\alpha, \beta}(\mathbf{x}_i, \mathbf{y}_i). \end{aligned} \quad (15)$$

By minimizing  $\hat{J}_{GCL}(\mathbf{X}, \mathbf{Y})$ , (15) can be regarded as a cost function similar to the mean square error criterion. It is worth pointing out that compared with the conventional Kalman filtering method based on the MSE criterion, the GCL criterion can deal with the non-Gaussian noise effectively, which owns strong robustness against outliers.

#### B. GCL Strategy Based on CKF

As a typical Kalman filter for processing nonlinear models, the CKF algorithm is mainly composed of two parts as follows.

1) **State Prediction:** First, suppose that a set of  $n$ -dimensional state variables  $\mathbf{X}_0$  is given at the initial time instant, then the initial state mean  $\hat{\mathbf{X}}_{0|0} = E[\mathbf{X}_0]$  and state error covariance  $\mathbf{P}_{0|0}$  can be represented by

$$\mathbf{P}_{0|0} = E\left[(\mathbf{X}_0 - \hat{\mathbf{X}}_{0|0})(\mathbf{X}_0 - \hat{\mathbf{X}}_{0|0})^T\right]. \quad (16)$$

By utilizing the state estimation value  $\hat{\mathbf{X}}_{k-1|k-1}$  and the Cholesky decomposition of the state error covariance  $\mathbf{P}_{k-1|k-1}$  at time instant  $k-1$ , a set of cubature points  $\mathbf{X}_{i, k-1|k-1}$  and  $\mathbf{X}_{i, k|k-1}^*$  are generated by

$$\mathbf{P}_{k-1|k-1} = \mathbf{S}_{k-1|k-1} \mathbf{S}_{k-1|k-1}^T, \quad (17)$$

$$\mathbf{X}_{i, k-1|k-1} = \mathbf{S}_{k-1|k-1} \xi_i + \hat{\mathbf{X}}_{k-1|k-1}, \quad \text{for } i=1, \dots, 2n \quad (18)$$

$$\mathbf{X}_{i, k|k-1}^* = \phi(\mathbf{X}_{i, k-1|k-1}, \mathbf{u}_k), \quad (19)$$

where  $\xi_i$  represents the  $i$ -th cubature point of the cubature point set  $\{\xi_i\}$  ( $i=1, 2, \dots, 2n$ ), and  $n$  is the number of state variables, the form of  $\xi_i$  is defined as follows

$$\{\xi_i\} = \sqrt{n} \begin{bmatrix} \begin{bmatrix} 1 \\ 0 \\ \vdots \\ 0 \end{bmatrix} & \begin{bmatrix} 0 \\ 0 \\ \vdots \\ 1 \end{bmatrix} & \begin{bmatrix} -1 \\ 0 \\ \vdots \\ 0 \end{bmatrix} & \begin{bmatrix} 0 \\ 0 \\ \vdots \\ -1 \end{bmatrix} \end{bmatrix}. \quad (20)$$

Then, the prior state prediction  $\hat{\mathbf{X}}_{k|k-1}$  and covariance prediction  $\mathbf{P}_{k|k-1}$  at time instant  $k-1$  can be calculated by

$$\hat{\mathbf{X}}_{k|k-1} = \frac{1}{2n} \sum_{i=1}^{2n} \mathbf{X}_{i, k|k-1}^*, \quad (21)$$

$$\mathbf{P}_{k|k-1} = \frac{1}{2n} \sum_{i=1}^{2n} \mathbf{X}_{i, k|k-1}^* \mathbf{X}_{i, k|k-1}^{*\top} - \hat{\mathbf{X}}_{k|k-1} \hat{\mathbf{X}}_{k|k-1}^T + \mathbf{Q}_{k-1}. \quad (22)$$

2) **Measurement Update:** By Cholesky decomposition of  $\mathbf{P}_{k|k-1}$ , a set of equal-weight cubature points  $\mathbf{X}_{i, k|k-1}$  around the state prediction value  $\hat{\mathbf{X}}_{k|k-1}$  can be generated as follows

$$\mathbf{P}_{k|k-1} = \mathbf{S}_{k|k-1} \mathbf{S}_{k|k-1}^T, \quad (23)$$

$$\mathbf{X}_{i,k|k-1} = \mathbf{S}_{k|k-1} \xi_i + \widehat{\mathbf{X}}_{k|k-1}, \quad \text{for } i=1, \dots, 2n \quad (24)$$

$$\mathbf{Z}_{i,k|k-1} = \mathbf{h}(\mathbf{X}_k^m, \mathbf{X}_{i,k|k-1}). \quad (25)$$

The prior measurement mean  $\widehat{\mathbf{Z}}_{k|k-1}$  and cross-covariance  $\mathbf{P}_{xz,k|k-1}$  between the states and measurements can be derived as

$$\widehat{\mathbf{Z}}_{k|k-1} = \frac{1}{2n} \sum_{i=1}^{2n} \mathbf{Z}_{i,k|k-1}, \quad (26)$$

$$\mathbf{P}_{xz,k|k-1} = \frac{1}{2n} \sum_{i=1}^{2n} \mathbf{X}_{i,k|k-1} \mathbf{Z}_{i,k|k-1}^T - \widehat{\mathbf{X}}_{k|k-1} \widehat{\mathbf{Z}}_{k|k-1}^T. \quad (27)$$

**3) State Update:** In order to make full use of the conducive characteristics of GCL criterion against the non-Gaussian noise, the nonlinear regression method based on GCL is derived in this section, which intends to approximate the nonlinear model of actual power system exactly and can be developed by the following procedure.

At first, based on the nonlinear power system model expressed by (5), the following equation can be derived:

$$\begin{bmatrix} \widehat{\mathbf{X}}_{k|k-1} \\ \mathbf{Z}_k \end{bmatrix} = \begin{bmatrix} \mathbf{X}_k \\ \mathbf{h}(\mathbf{X}_k^m, \mathbf{X}_k) \end{bmatrix} + \begin{bmatrix} \boldsymbol{\psi}_k(\mathbf{X}_k) \\ \mathbf{v}_k \end{bmatrix}, \quad (28)$$

where  $\boldsymbol{\psi}_k(\mathbf{X}_k) = \mathbf{X}_k - \widehat{\mathbf{X}}_{k|k-1}$ , and defined as follows

$$\boldsymbol{\xi}_k = \begin{bmatrix} -\boldsymbol{\psi}_k(\mathbf{X}_k) \\ \mathbf{v}_k \end{bmatrix}, \quad (29)$$

with

$$\begin{aligned} E \begin{bmatrix} \boldsymbol{\xi}_k \boldsymbol{\xi}_k^T \\ \boldsymbol{\xi}_k \zeta_k^T \end{bmatrix} &= \begin{bmatrix} \mathbf{P}_{k|k-1} & 0 \\ 0 & \mathbf{R}_k \end{bmatrix} = \begin{bmatrix} \mathbf{B}_{p,k|k-1} \mathbf{B}_{p,k|k-1}^T & 0 \\ 0 & \mathbf{B}_{r,k} \mathbf{B}_{r,k}^T \end{bmatrix} \\ &= \begin{bmatrix} \mathbf{B}_{p,k|k-1} & 0 \\ 0 & \mathbf{B}_{r,k} \end{bmatrix} \begin{bmatrix} \mathbf{B}_{p,k|k-1} & 0 \\ 0 & \mathbf{B}_{r,k} \end{bmatrix}^T = \mathbf{B}_k \mathbf{B}_k^T, \quad (30) \end{aligned}$$

where  $\mathbf{B}_k$  can be obtained by Cholesky decomposition of  $E \begin{bmatrix} \boldsymbol{\xi}_k \boldsymbol{\xi}_k^T \\ \boldsymbol{\xi}_k \zeta_k^T \end{bmatrix}$ . In order to facilitate the solution, both sides of (26) are multiplied by  $\mathbf{B}_k^{-1}$  at the same time instant, the nonlinear regression model based on the generalized correntropy loss can be further be described as

$$\mathbf{D}_k = \mathbf{F}_k(\mathbf{X}_k) + \boldsymbol{\gamma}_k, \quad (31)$$

where

$$\begin{aligned} \mathbf{D}_k &= \mathbf{B}_k^{-1} \begin{bmatrix} \widehat{\mathbf{X}}_{k|k-1} \\ \mathbf{Z}_k \end{bmatrix}, \quad \mathbf{F}_k(\mathbf{X}_k) = \mathbf{B}_k^{-1} \begin{bmatrix} \mathbf{X}_k \\ \mathbf{h}(\mathbf{X}_k^m, \mathbf{X}_k) \end{bmatrix} \\ \boldsymbol{\gamma}_k &= \mathbf{B}_k^{-1} \begin{bmatrix} -(\mathbf{X}_k - \widehat{\mathbf{X}}_{k|k-1}) \\ \mathbf{v}_k \end{bmatrix} = \mathbf{B}_k^{-1} \boldsymbol{\xi}_k, \quad (32) \end{aligned}$$

with

$$\begin{aligned} E \begin{bmatrix} \boldsymbol{\gamma}_k \boldsymbol{\gamma}_k^T \\ \boldsymbol{\gamma}_k \zeta_k^T \end{bmatrix} &= E \begin{bmatrix} \mathbf{B}_k^{-1} \boldsymbol{\xi}_k \boldsymbol{\xi}_k^T (\mathbf{B}_k^{-1})^T \\ \mathbf{B}_k^{-1} \boldsymbol{\xi}_k \zeta_k^T (\mathbf{B}_k^{-1})^T \end{bmatrix} \\ &= E \begin{bmatrix} \mathbf{B}_k^{-1} \mathbf{B}_k \mathbf{B}_k^T (\mathbf{B}_k^{-1})^T \\ \mathbf{B}_k^{-1} \mathbf{I} \end{bmatrix} = E \begin{bmatrix} \mathbf{I} \\ \mathbf{I} \end{bmatrix} = \mathbf{I}, \quad (33) \end{aligned}$$

where  $\mathbf{I}$  symbolizes the identity matrix.

Subsequently, the cost function based on the GCL criterion can be constructed as follows

$$\widehat{\mathbf{J}}_{GCL}(\mathbf{X}_i) = \xi_{\alpha, \beta} \left[ 1 - \frac{1}{L} \sum_{k=1}^L \exp \left\{ -\varphi |\boldsymbol{\gamma}_{i,k}|^\alpha \right\} \right], \quad (34)$$

where  $L = n + m$ ,  $m$  is the dimension of the measured variable;  $\boldsymbol{\gamma}_{i,k} = \mathbf{D}_{i,k} - \mathbf{F}_{i,k}(\mathbf{X}_{i,k})$ ,  $\boldsymbol{\gamma}_{i,k}$  denotes the  $i$ -th element of matrix  $\boldsymbol{\gamma}_k$ . According to the cost function  $\widehat{\mathbf{J}}_{GCL}(\mathbf{X}_i)$ , the optimal state variable  $\widehat{\mathbf{X}}_i$  can be calculated by

$$\widehat{\mathbf{X}}_i = \arg \min_{\mathbf{X}_i} \xi_{\alpha, \beta} \left[ 1 - \frac{1}{L} \sum_{k=1}^L \exp \left\{ -\varphi |\boldsymbol{\gamma}_{i,k}|^\alpha \right\} \right]. \quad (35)$$

Accordingly, let  $\partial \widehat{\mathbf{J}}_{GCL}(\mathbf{X}_i) / \partial \mathbf{X}_i = 0$ , the following equation can be obtained

$$\left( \frac{\partial \mathbf{F}_k(\mathbf{X}_k)}{\partial \mathbf{X}_k} \right)^T \mathbf{U}_k (\mathbf{D}_k - \mathbf{F}_k(\mathbf{X}_k)) = 0, \quad (36)$$

where

$$\mathbf{U}_k = \begin{bmatrix} \mathbf{U}_{x,k} & 0 \\ 0 & \mathbf{U}_{z,k} \end{bmatrix}, \quad (37)$$

with  $\mathbf{U}_{x,k} = \text{diag}(\mathbf{g}_\beta(\boldsymbol{\gamma}_{1,k}), \dots, \mathbf{g}_\beta(\boldsymbol{\gamma}_{n,k}))$ ,  $\mathbf{U}_{z,k} = \text{diag}(\mathbf{g}_\beta(\boldsymbol{\gamma}_{n+1,k}), \dots, \mathbf{g}_\beta(\boldsymbol{\gamma}_{n+m,k}))$ ,  $\mathbf{g}_\beta(\boldsymbol{\gamma}_{k,i}) = \exp \left\{ -\varphi |\boldsymbol{\gamma}_{k,i}|^\alpha \right\} |\boldsymbol{\gamma}_{k,i}|^{\alpha-2}$ .

It is worth pointing out that when the measurement is corrupted by the non-Gaussian noise, the correntropy gain  $\mathbf{U}_k$  will be reduced to zero, which can avoid the divergence of state estimation effectively.

In order to facilitate the iterative calculation dynamically, (35) can be further derived as a fixed-point iterative form as follows

$$\begin{aligned} \widehat{\mathbf{X}}_k^{(r)} &= \left( \Theta^T(\widehat{\mathbf{X}}_k^{(r-1)}) \mathbf{U}_k^{(r-1)} \Theta(\widehat{\mathbf{X}}_k^{(r-1)}) \right)^{-1} \Theta^T(\widehat{\mathbf{X}}_k^{(r-1)}) \mathbf{U}_k^{(r-1)} \\ &\quad \times \left( \Theta(\widehat{\mathbf{X}}_k^{(r-1)}) - \phi(\widehat{\mathbf{X}}_k^{(r-1)}) + \mathbf{z}_k \right), \quad (38) \end{aligned}$$

where  $\Theta(\widehat{\mathbf{X}}_k^{(r-1)}) = \left. \frac{\partial \mathbf{F}_k(\mathbf{X}_k)}{\partial \mathbf{X}_k} \right|_{\mathbf{X}=\widehat{\mathbf{X}}_k^{(r-1)}}$ .

Then, by weighting the residuals with correntropy gain  $\mathbf{U}_k$ , the prediction covariance  $\mathbf{P}_{k|k-1}$  and the measurement noise  $\mathbf{R}_k$  can be corrected by

$$\widetilde{\mathbf{P}}_{k|k-1} = \mathbf{B}_{p,k|k-1} \mathbf{U}_{x,k}^{-1} \mathbf{B}_{p,k|k-1}^T, \quad (39)$$

$$\widetilde{\mathbf{R}}_k = \mathbf{B}_{r,k} \mathbf{U}_{y,k}^{-1} \mathbf{B}_{r,k}^T. \quad (40)$$

Thus, (36) can be further transformed into the following form

$$\widehat{\mathbf{X}}_{k|k} = \widehat{\mathbf{X}}_{k|k-1} + \mathbf{K}_k (\mathbf{Z}_k - \widehat{\mathbf{Z}}_{k|k-1}), \quad (41)$$

where  $\mathbf{K}_k = \mathbf{P}_{xz,k|k-1} \mathbf{P}_{zz,k|k-1}^{-1}$  represents the gain matrix. Then, the posterior state error covariance can be updated as follows

$$\mathbf{P}_{k|k} = \widetilde{\mathbf{P}}_{k|k-1} - \mathbf{K}_k \mathbf{P}_{zz,k|k-1} \mathbf{K}_k^T, \quad (42)$$

where  $\mathbf{P}_{zz,k|k-1} = \frac{1}{2n} \sum_{i=1}^{2n} \mathbf{Z}_{i,k|k-1} \mathbf{Z}_{i,k|k-1}^T - \widehat{\mathbf{Z}}_{k|k-1} \widehat{\mathbf{Z}}_{k|k-1}^T + \widetilde{\mathbf{R}}_k$ .

It is worth noting that in order to prevent the singularity of matrix  $U_k$  caused by the sharp increase of measurement information, the following means are utilized

$$\zeta_k = Z_k - \hat{Z}_{k|k-1}, \quad (43)$$

$$\eta_k = P_{zz,k|k-1}, \quad (44)$$

$$\tau_k = \zeta_k^T \eta_k^{-1} \zeta_k, \quad (45)$$

where  $\varpi$  is a positive threshold and should be set in advance. While  $|\tau_k| > \varpi$ , only the time update step without states update step is executed, i.e.,  $\hat{X}_{k|k} = \hat{X}_{k|k-1}$  and  $P_{k|k} = P_{k|k-1}$ . Otherwise, both are worked.

### C. Adaptive Kernel Bandwidth

From (12), it should be pointed out that the efficacy of the method based on correntropy criterion is significantly affected by the kernel bandwidth. To be specific, if a too large kernel bandwidth is utilized, the ability of the estimator against outliers can be degraded heavily; on the contrary, if a too small kernel bandwidth is used, the estimation accuracy and convergence speed of the estimator will be severely reduced [31]. Therefore, the selection of an appropriate kernel bandwidth is very important to ensure the performance of the proposed method. To deal with the above issue and acquire the suitable kernel bandwidth, an adaptive factor  $\mu_k$  is introduced to achieve the optimal kernel bandwidth adaptively.

Let  $d_k = tr(P_{zz,k|k-1}) - tr(\zeta_k \zeta_k^T)$  primarily. Then, by comparing the trace of prior measurement covariance  $P_{zz,k|k-1}$  with that of the innovation vector  $\zeta_k \zeta_k^T$  proposed in (42). Thereby, the adaptive factor  $\mu_k$  can be defined as

$$\mu_k = \begin{cases} 1 & \text{if } d_k > 0, \\ \frac{tr(P_{zz,k|k-1})}{tr(\zeta_k \zeta_k^T)} & \text{otherwise,} \end{cases} \quad (46)$$

where  $tr(A)$  represents the trace of  $A$ .

Therefore, the kernel bandwidth  $\beta$  can be calculated by

$$\beta_k = \beta_{k-1} \mu_k. \quad (47)$$

Note that when lots of abnormal data appear in the measured information, it can be seen from (43) that the innovation vector  $\zeta_k$  become larger, and then the  $d_k$  will be less than or equal to zero. Further, adjusted by the adaptive factor  $\mu_k$  in (47), the kernel bandwidth will be dynamically updated corresponding to the changing measurement information.

**Remark 1:** As described in [32], the kernel function with an inappropriate kernel bandwidth will seriously affect the filtering performance of the estimator. In addition, the fixed-size kernel bandwidth is adopted by [27], which is usually obtained based on a large number of experiments and debugging. Therefore, it is troublesome to accurately select an appropriate kernel bandwidth with varying measurement information.

**Remark 2:** In order to solve the above problem, an adaptive correction technology is developed in (46). By utilizing this

methodology, the kernel bandwidth can be adjusted dynamically and adaptively with the actual operating conditions of the power system, where not only the difficulty in choosing the appropriate kernel bandwidth is avoided, but also a much better estimation performance can be achieved.

For convenience, the proposed AGCLCKF approach for robust dynamic state estimation of power system is fully summarized as **Algorithm 1**:

#### Algorithm 1: AGCLCKF with Nonlinear Regression

**Step 1:** Initialization:  $k = 1, \beta, \varepsilon, \hat{X}_{0|0}, \hat{P}_{0|0}, Q_{k-1}, R_k, \varpi$

**Step 2:** Time update:

A set of cubature points  $X_{i,k-1|k-1}$  and  $X_{i,k-1}^*$  are obtained by (17) – (19), and then the prior state prediction  $\hat{X}_{k|k-1}$  and  $P_{k|k-1}$  are calculated by (21) – (22).

**Step 3:** Measurement update:

The cubature points  $X_{i,k|k-1}$  and  $Z_{i,k|k-1}$  and the prior measurements  $\hat{Z}_{k|k-1}$  and  $P_{zz,k|k-1}$  are obtained by (23) – (25) and (26) – (27), respectively.

**If**  $|\tau_k| > \varpi$  **then**

$$\hat{X}_{k|k} = \hat{X}_{k|k-1} \text{ and } P_{k|k} = P_{k|k-1}$$

**else**

**Step 4:** Initialization:  $t = 1, \hat{X}_{k|k}^{(0)} = \hat{X}_{k|k-1}$  and  $\beta_{k,0} = \beta_{k-1}$

**Repeat:**

Update the states  $\hat{X}_{k|k}^{(t)}$  and the state error covariance  $P_{k|k}^{(t)}$  according to (41)-(42)

$$K_k^{(t-1)} = P_{xz,k|k-1} (P_{zz,k|k-1}^{(t-1)})^{-1}$$

$$\hat{X}_{k|k}^{(t)} = \hat{X}_{k|k-1} + K_k^{(t-1)} (Z_k - \hat{Z}_{k|k-1})$$

$$P_{k|k}^{(t)} = \tilde{P}_{k|k-1}^{(t-1)} - K_k^{(t-1)} P_{zz,k|k-1}^{(t-1)} (K_k^{(t-1)})^T$$

where the prediction covariance  $\tilde{P}_{k|k-1}^{(t-1)}$ ,  $P_{zz,k|k-1}^{(t-1)}$  and measurement noise  $\tilde{R}_k^{(t-1)}$  corrected by correntropy gain  $U_k$  can be obtained by

$$\tilde{P}_{k|k-1}^{(t-1)} = B_{p,k|k-1} (U_{x,k}^{(t-1)})^{-1} B_{p,k|k-1}^T$$

$$P_{zz,k|k-1}^{(t-1)} = \frac{1}{2n} \sum_{i=1}^{2n} Z_{i,k|k-1} Z_{i,k|k-1}^T - \hat{Z}_{k|k-1} \hat{Z}_{k|k-1}^T + \tilde{R}_k^{(t-1)}$$

$$\tilde{R}_k^{(t-1)} = B_{r,k} (U_{z,k}^{(t-1)})^{-1} B_{r,k}^T$$

with

$$U_{x,k}^{(t-1)} = \text{diag} \left( g_\beta \left( \gamma_{1,k}^{(t-1)} \right), \dots, g_\beta \left( \gamma_{n,k}^{(t-1)} \right) \right)$$

$$U_{z,k}^{(t-1)} = \text{diag} \left( g_\beta \left( \gamma_{n+1,k}^{(t-1)} \right), \dots, g_\beta \left( \gamma_{n+m,k}^{(t-1)} \right) \right)$$

$$g_\beta \left( \gamma_{i,k}^{(t-1)} \right) = \exp \left\{ -\varphi \left| \gamma_{i,k}^{(t-1)} \right|^a \right\} \left| \gamma_{i,k}^{(t-1)} \right|^{a-2}$$

$$\gamma_{i,k}^{(t-1)} = D_{i,k} - F_{i,k} \left( \hat{X}_{k|k}^{(t-1)} \right)$$

**Step 5:** Correct kernel bandwidth  $\beta_k$  of GCL by adaptive factor  $\mu_k$ :

$$\begin{aligned} \mathbf{P}_{k|k}^{(t)} &= \mathbf{S}_{k|k}^{(t)} (\mathbf{S}_{k|k}^{(t)})^T, \mathbf{X}_{i,k|k}^{(t)} = \mathbf{S}_{k|k}^{(t)} \xi_i + \widehat{\mathbf{X}}_{k|k}^{(t)} \text{ for } i=1, \dots, 2n \\ \mathbf{Z}_{i,k|k}^{(t)} &= \mathbf{h}(\mathbf{X}_{i,k}^m, \mathbf{X}_{i,k|k}^{(t)}), \widehat{\mathbf{Z}}_{k|k}^{(t)} = \frac{1}{2n} \sum_{i=1}^{2n} \mathbf{Z}_{i,k|k}^{(t)}, \\ \zeta_k^{(t)} &= \mathbf{Z}_k - \widehat{\mathbf{Z}}_{k|k}^{(t)}, d_k^t = \text{tr}(\mathbf{P}_{z,z,k|k-1}) - \text{tr}(\zeta_k^{(t)} (\zeta_k^{(t)})^T) \\ \mu_k^t &= \begin{cases} 1 & \text{if } d_k^t > 0, \\ \frac{\text{tr}(\mathbf{P}_{z,z,k|k-1})}{\text{tr}(\zeta_k^t (\zeta_k^t)^T)} & \text{otherwise,} \end{cases} \\ \beta_k^t &= \beta_{k-1}^t \mu_k^t \end{aligned}$$

**Step 6:**  $t = t + 1$

$$\text{Until } \frac{\|\widehat{\mathbf{X}}_{k|k}^{(t)} - \widehat{\mathbf{X}}_{k|k}^{(t-1)}\|}{\|\widehat{\mathbf{X}}_{k|k}^{(t-1)}\|} \leq \varepsilon$$

where  $\varepsilon$  is a positive threshold, which indicates that the internal iteration will be stopped.

**End**

**Step 7:**  $k = k + 1$ , go back to **Step 2**.

#### IV. ILLUSTRATIVE EXAMPLE

In this section, extensive simulations are carried out on the New England test system model with 10 generators and 39 buses to demonstrate the effectiveness and robustness of the proposed method under various conditions. The single-line diagram of the test system and its detailed parameters can be found in [21]. By utilizing the software PSCAD/EMTDC<sup>®</sup>, the true state variables and measurements can be generated to simulate transient stability. Note that the input variables of system are usually treated as known. The specific verification includes the following steps: when  $t = 0.5 \text{ s}$ , a three-phase grounding fault suddenly occurs at the line outlet of bus 16-bus 21, which is solved at  $t = 0.7 \text{ s}$ . The sampling frequency of the phasor measurement unit is 50 samples per second. Then,  $N_{MC} = 200$  independent Monte-Carlo simulations are carried out for each case study to acquire more reliable statistical significance. In the following discussion, the generator 2 (G2) is randomly taken as an example. All the tests are implemented in Matlab environment using Intel<sup>®</sup> Core TM i5 2.30GHz CPU with 16GB memory computer.

In order to visualize and digitize the statistical results, the overall performance index  $E_x$  and the mean absolute error (MAE) in [21] are used to evaluate the performance of various algorithms, which are defined as

$$\text{MAE}(k) = \frac{1}{N_{MC}} \sum_{i=1}^{N_{MC}} \frac{1}{N_S} \sum_{s=1}^{N_S} |X_{i,k} - \widehat{X}_{i,k}|, \quad (48)$$

$$E_x = \frac{1}{N_{MC}} \sum_{i=1}^{N_{MC}} \sqrt{\sum_{k=1}^{N_T} (X_{i,k} - \widehat{X}_{i,k})^2 / N_T}, \quad (49)$$

where  $N_{MC}$ ,  $N_S$  and  $N_T$  represent the total number of Monte Carlo runs, state variables and simulation time, respectively;  $X_{i,k}$  and  $\widehat{X}_{i,k}$  denote the true and estimated value of states, respectively.

In order to verify and highlight the efficacy of the proposed method, the methods CKF [11], HCKF [35], and the developed GCLCKF are utilized to make comparisons under the different circumstances.

##### A. Case I: Gaussian Noise Distribution Conditions

In this subsection, it is assumed that the noise statistics of the system model obey the following Gaussian distribution:  $\mathbf{Q}_k = 10^{-6} \mathbf{I}$  and  $\mathbf{R}_k = 10^{-5} \mathbf{I}$ , which represents the state and measurement error covariance matrix, respectively; and both of them are zero mean. The shape parameter  $\alpha$  is set as 1.9. The initial state covariance  $\mathbf{P}_0 = 10^{-5} \mathbf{I}$ .

In this case, the overall performance  $E_x$  of CKF [11], HCKF [35], GCLCKF and AGCLCKF for various states of generator are shown in TABLE I. It can be easily noted that the  $E_x$  of GCLCKF and AGCLCKF is much smaller than that of CKF and HCKF. In addition, compared with the CKF, the overall performance index of HCKF is smaller. By introducing robust control theory, the system and measurement noise statistics can be dynamically modified, so that the HCKF method can achieve superior performance than the conventional CKF in this case.

More importantly, the proposed AGCLCKF can achieve better estimation performance than GCLCKF due to the adaptive adjustment of the kernel bandwidth. Meanwhile, those results also clarify that the size of kernel bandwidth will affect the filtering performance of GCLCKF and AGCLCKF obviously. As shown in Table I, it can be seen that when  $\beta$  is set as 3, GCLCKF and AGCLCKF have relatively minimal errors. Note that this kernel bandwidth is adopted in the following discussion.

TABLE I  
OVERALL PERFORMANCE  $E_x$  OF  $\delta$ ,  $\omega$ ,  $e'_q$  AND  $e'_d$   
WITH THE GAUSSIAN NOISE

Filter	$E_x$ of $\delta$	$E_x$ of $\omega$	$E_x$ of $e'_q$	$E_x$ of $e'_d$
CKF	0.0296	0.2970	0.2175	0.7212
HCKF	0.0110	0.0241	0.1236	0.4161
GCLCKF ( $\beta=2$ )	$0.113 \times 10^{-3}$	$0.665 \times 10^{-3}$	0.0222	0.0450
GCLCKF ( $\beta=3$ )	$0.120 \times 10^{-3}$	$0.614 \times 10^{-3}$	0.0214	0.0241
GCLCKF ( $\beta=5$ )	$0.122 \times 10^{-3}$	$0.609 \times 10^{-3}$	0.0242	0.0366
GCLCKF ( $\beta=10$ )	$0.124 \times 10^{-3}$	$0.635 \times 10^{-3}$	0.0233	0.0451
AGCLCKF ( $\beta=2$ )	$0.079 \times 10^{-3}$	$0.186 \times 10^{-3}$	0.0151	0.0439
AGCLCKF ( $\beta=3$ )	$0.077 \times 10^{-3}$	$0.158 \times 10^{-3}$	0.0102	0.0225
AGCLCKF ( $\beta=5$ )	$0.085 \times 10^{-3}$	$0.161 \times 10^{-3}$	0.035	0.0343
AGCLCKF ( $\beta=10$ )	$0.084 \times 10^{-3}$	$0.169 \times 10^{-3}$	0.016	0.0554

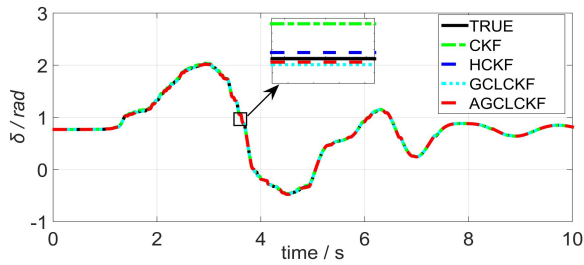


Fig. 1. Estimation results of  $\delta$  for G2 with the Gaussian noise.

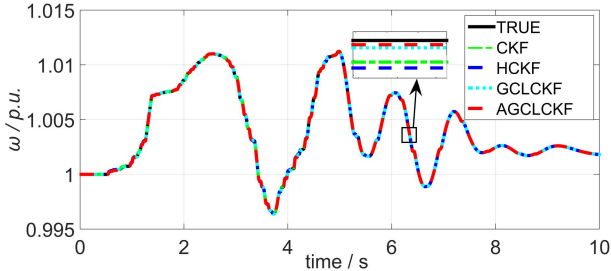


Fig. 2. Estimation results of  $\omega$  for G2 with the Gaussian noise.

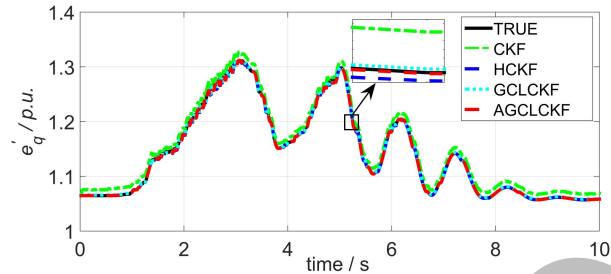


Fig. 3. Estimation results of  $e'_q$  for G2 with the Gaussian noise.

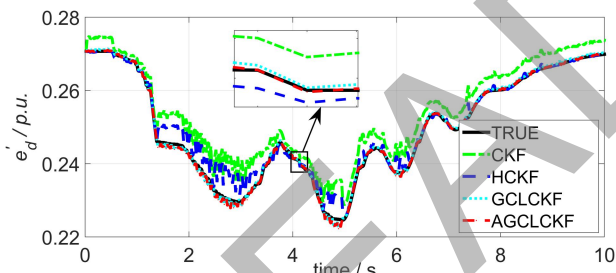


Fig. 4. Estimation results of  $e'_d$  for G2 with the Gaussian noise.

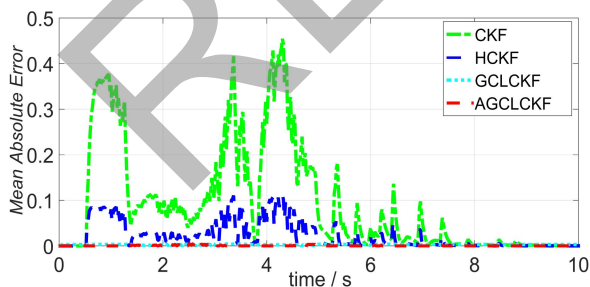


Fig. 5. MAE results of each approach for G2 with the Gaussian noise.

Next, the estimated results of G2 are taken for illustration. Figs. 1-4 show the estimated results of the different discussed methods with the Gaussian noise. It can be observed that compared with CKF and HCKF, GCLCKF and AGCLCKF

are more accurate in state tracking, especially for the state variables  $e'_q$  and  $e'_d$ . Moreover, due to the correction of kernel bandwidth, the proposed AGCLCKF performs better than GCLCKF slightly. In contrast, the performance of the CKF and HCKF methods is relatively poor in tracking the true states. Under this working condition, the average absolute error (MAE) results of the discussed methods for G2 are presented in Fig. 5, which are calculated from 200 Monte-Carlo runs. It can be noted that the MAE of CKF is the largest, followed by HCKF, GCLCKF is even smaller, and AGCLCKF has the smallest. In other words, the proposed AGCLCKF method can achieve the best estimation performance under the Gaussian noise distribution conditions.

### B. Case 2: Non-Gaussian Measurement Noise Conditions

Due to communication noise and external interference, the actual measurement noise measured by the PMU tends to deviate from the Gaussian noise. In order to verify the effectiveness of the proposed method under this condition, it is assumed that the measurement noise obeys the heavy-tailed non-Gaussian noise, which is generated by the mixed-Gaussian distribution such as [30]

$$r_k \sim (1-\theta)N(0, v_1^2) + \theta N(0, v_2^2),$$

where  $N(0, v_i^2)$  represents the Gaussian noise with zero mean and the covariance of  $v_i^2 (i=1,2)$ ;  $\theta$  indicates the degree of mixture. In this case study, the measured noise covariance  $v_i^2 (i=1,2)$  and the mixing parameter  $\theta$  are set to  $v_1=10^{-5}$ ,  $v_2=10^{-6}$  and  $\theta=0.1$ , respectively.

The estimated results of the proposed AGCLCKF method and other discussed approaches at each time instant  $k$  are displayed in Figs. 6-9. And the MAE results of 200 Monte-Carlo sampling of each method are further displayed in Fig. 10. It can be seen that the estimated result of CKF has seriously deviated from the true value of states under the non-Gaussian measurement noise circumstance. By utilizing the H-infinity theory, the performance of HCKF performs better than that of CKF to some extent. However, compared with GCL criterion, HCKF still has large error. In addition, it can be found that the tracking speed of AGCLCKF on state variables is significantly better than GCLCKF in this scenario, which is due to the correction of kernel bandwidth by adaptive factor  $\mu_k$ . Therefore, the AGCLCKF approach can achieve a higher filtering accuracy and more robust performance than the GCLCKF.

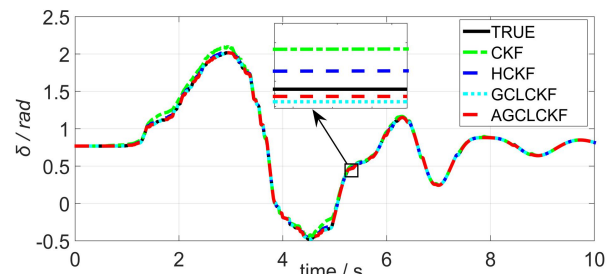


Fig. 6. Estimation results of  $\delta$  for G2 with the non-Gaussian measurement noise.

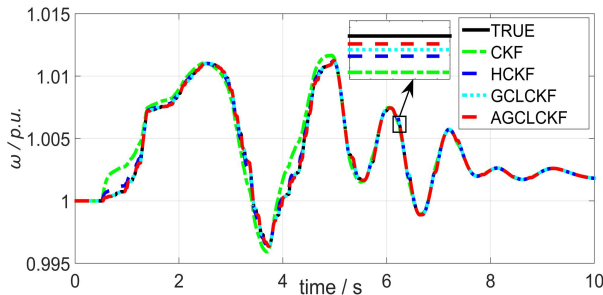


Fig. 7. Estimation results of  $\omega$  for G2 with the non-Gaussian measurement noise.

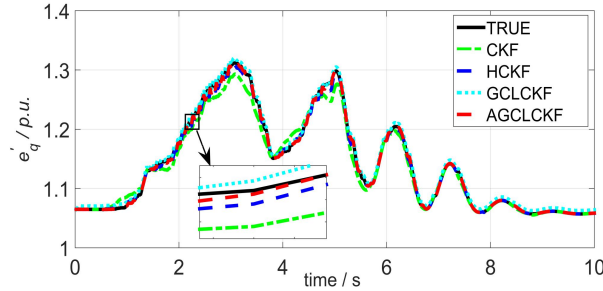


Fig. 8. Estimation results of  $e'_q$  for G2 with the non-Gaussian measurement noise.

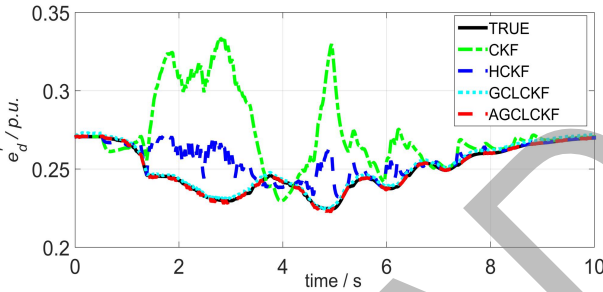


Fig. 9. Estimation results of  $e'_d$  for G2 with the non-Gaussian measurement noise.

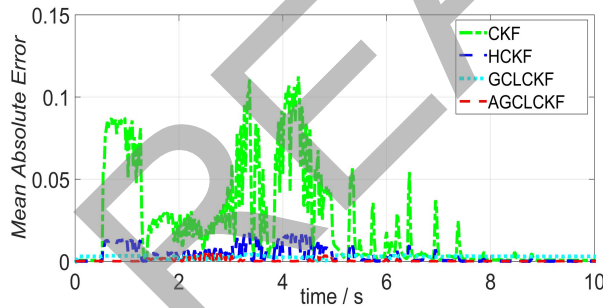


Fig. 10. MAE results of each approach for G2 with the non-Gaussian measurement noise.

Furthermore, the overall performance index  $E_x$  of the discussed approaches for each state are presented in TABLE II. As can be seen from it, the estimation error of CKF is the largest, followed by HCKF and GCLCKF. Besides, under the premise of a suitable kernel width, the AGCLCKF will achieve the smallest error result. In short, compared with other methods, the AGCLCKF has the optimal estimation accuracy and robustness under the non-Gaussian noise conditions.

TABLE II

OVERALL PERFORMANCE  $E_x$  OF  $\delta$ ,  $\omega$ ,  $e'_q$  AND  $e'_d$  WITH THE NON-GAUSSIAN MEASUREMENT NOISE

Filter	$E_x$ of $\delta$	$E_x$ of $\omega$	$E_x$ of $e'_q$	$E_x$ of $e'_d$
CKF	0.0096	0.0727	0.2389	0.6775
HCKF	0.0018	0.0113	0.0258	0.1533
GCLCKF ( $\beta=2$ )	0.0014	0.0095	0.0116	0.0586
GCLCKF ( $\beta=3$ )	0.0012	0.0065	0.0103	0.0477
GCLCKF ( $\beta=5$ )	0.0013	0.0063	0.0107	0.0496
GCLCKF ( $\beta=10$ )	0.0021	0.0077	0.0124	0.0487
AGCLCKF ( $\beta=2$ )	0.0010	0.0035	0.0098	0.0307
AGCLCKF ( $\beta=3$ )	0.0008	0.0028	0.0086	0.0211
AGCLCKF ( $\beta=5$ )	0.0013	0.0039	0.0093	0.0330
AGCLCKF ( $\beta=10$ )	0.0011	0.0105	0.0105	0.0423

### C. Case 3: Unknown Model Parameter Variation Conditions

In the actual power system, the uncertainties of the generators come not only from the complex non-Gaussian distributed noises, but also from the time-varying model parameters, which is due to the fluctuation of the mechanical characteristics, temperature, and the interference of saturation on the inductance, thus some parameters of the synchronous generator can be deviated from the rated values gradually [22]. According to [36] in terms of model validation and calibration, it can be concluded that the various parameters of generator reflect different sensitivities to system disturbances. Therefore, in order to investigate the robustness of each discussed method under this circumstance, in this case, the transient reactances of  $d$ -axis and  $q$ -axis are assumed to be 15% deviated from the rated values, which can be simulated by a Gaussian random variable with zero mean and given error as standard deviation.

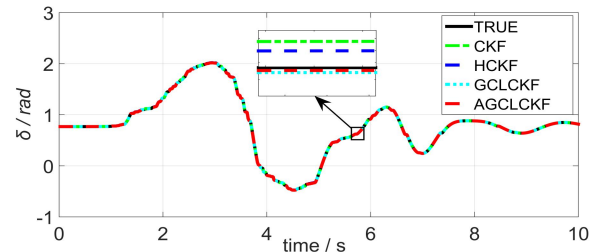


Fig. 11. Estimation results of  $\delta$  for G2 with model parameter variation.

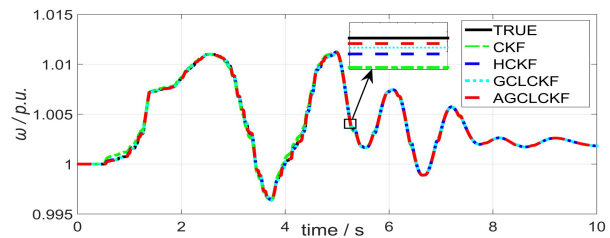


Fig. 12. Estimation results of  $\omega$  for G2 with model parameter variation.

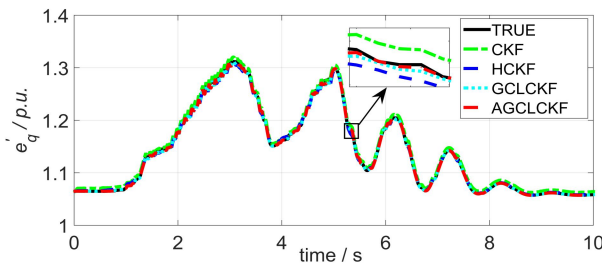


Fig. 13. Estimation results of  $e'_q$  for G2 with model parameter variation.

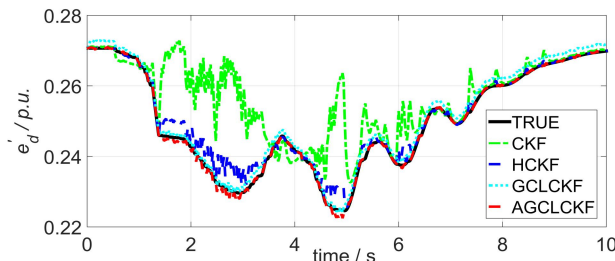


Fig. 14. Estimation results of  $e'_d$  for G2 with model parameter variation.

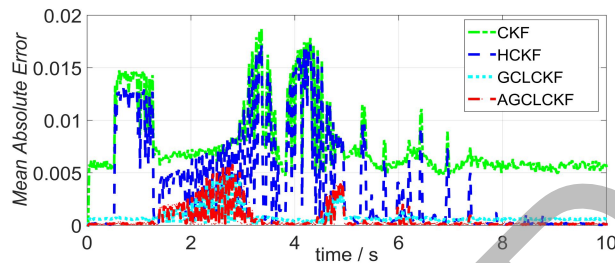


Fig. 15. MAE results of each approach for G2 with model parameter variation.

TABLE III  
OVERALL PERFORMANCE  $E_x$  OF  $\delta$ ,  $\omega$ ,  $e'_q$  AND  $e'_d$   
WITH MODEL PARAMETER VARIATION

Filter	$E_x$ of $\delta$	$E_x$ of $\omega$	$E_x$ of $e'_q$	$E_x$ of $e'_d$
CKF	0.0503	0.0153	0.0498	0.3843
HCKF	0.0321	0.0223	0.0363	0.1931
GCLCKF ( $\beta=2$ )	0.0211	0.0208	0.0222	0.1335
GCLCKF ( $\beta=3$ )	0.0106	0.0147	0.0107	0.1023
GCLCKF ( $\beta=5$ )	0.0117	0.0149	0.0110	0.1104
GCLCKF ( $\beta=10$ )	0.0134	0.0151	0.0523	0.1299
AGCLCKF ( $\beta=2$ )	0.0105	0.0123	0.0211	0.0995
AGCLCKF ( $\beta=3$ )	0.0099	0.0117	0.0069	0.0864
AGCLCKF ( $\beta=5$ )	0.0110	0.0125	0.0121	0.0902
AGCLCKF ( $\beta=10$ )	0.0127	0.0133	0.0438	0.0105

Figs. 11-14 display the state tracking of CKF, HCKF, GCLCKF, and AGCLCKF methods in the presence of unknown model parameter changes. In addition, the MAE

comparison results of various filters in this case are provided in Fig. 15. The  $E_x$  indices are calculated by 200 Monte-Carlo simulations for each of the discussed approaches are exhibited in TABLE III. It can be seen that all the discussed approaches can roughly estimate the states, the estimation results are significantly different. To be specific, as the CKF lacks the robustness against uncertainty, it cannot converge quickly, which is much sensitive to parameter fluctuations, especially for the state estimation of  $e'_d$ . Compared with the CKF, the MAE and  $E_x$  results of HCKF are slightly lower. In other words, the relatively stronger robustness is embodied in HCKF, due to the constraint of parameter variation to a certain extent. However, compared with the CKF and its variants, which use the minimum error criterion as the cost function, the GCL criterion owns stronger robustness. Based utilizing the GCL criterion, the GCLCKF can suppress the adverse effects caused by the uncertain transient reactance with fast convergence rate. Nevertheless, compared to the GCLCKF with a fixed kernel size, the AGCLCKF has smaller error results and more accurate filtering performance, which is due to the fact that it can dynamically adjust the covariance matrix and the bandwidth of kernel according to the changes of parameters.

#### D. Case 4: Evaluation of Computational Efficiency

For the dynamic state estimation of power system, the efficiency of algorithm is another paramount factor. Therefore, the overall calculation time of all the discussed methods in the Case 1-3 is fully investigated, which is shown in Fig. 16. It can be seen that the total calculation time of CKF, HCKF, GCLCKF, and the proposed AGCLCKF algorithms increase in turn. To be specific, the CKF takes the least time, followed by HCKF due to the adjustment of constraint parameter  $\gamma^2$  and the update of large-scale matrix. Moreover, the GCLCKF takes a little more time than HCKF, this is because it involves the tuning of the measurement noise  $R_k$  and the state covariance  $P_k$  with correntropy gain  $U_k$ . In addition, compared with the GCLCKF, due to the adaptive correction of the kernel bandwidth  $\beta_k$ , the AGCLCKF spent a little bit more calculation time. Nevertheless, it is still less than the sampling rate of the PMU (20 milliseconds, 50 samples per second). Therefore, the proposed filter AGCLCKF is able to achieve the real-time tracking of power system dynamic estimation online.

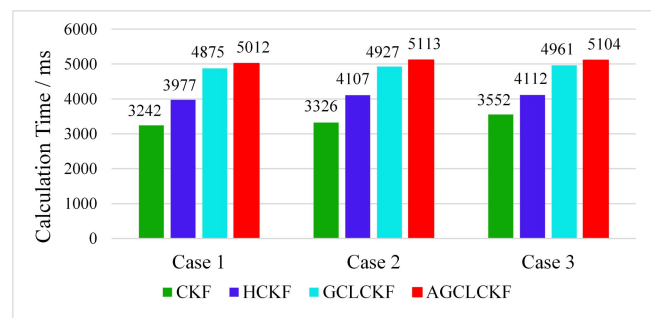


Fig. 16. Overall calculation time of all filters in the case studies 1-3

## V. CONCLUSION

To deal with the widespread non-Gaussian noise problem in the power system, a novel robust DSE strategy based on generalized correntropy loss criterion with CKF framework was proposed. In this method, by utilizing the GCL optimal criterion and nonlinear regression model, the error covariance and noise covariance are adjusted through the correntropy gain, where not only the susceptibility to the non-Gaussian noise in the measurement information can be greatly reduced, but also the strong nonlinearities can be addressed effectively so as to further improve the accuracy of estimation. In addition, to enhance the flexibility and robustness of the proposed method, an adaptive strategy is introduced to update the kernel bandwidth in real-time. Extensive numerical experiments carried out on IEEE 39-bus test system have verified the accuracy and robustness of the proposed AGCLCKF method for DSE in power system. In future work, we further consider applying the proposed filtering method to combined networks including transmission and distribution networks with renewable energy resources.

## REFERENCES

- [1] Y. Yu, Z. Wang and C. Lu, "A joint filter approach for reliable power system state estimation," *IEEE Trans. Instrum. Meas.*, vol. 68, no. 1, pp. 87-94, Jan. 2019.
- [2] B. Uzunoğlu and M. A. Ülker, "Maximum likelihood ensemble filter state estimation for power system," *IEEE Trans. Instrum. Meas.*, vol. 67, no. 9, pp. 2097-2106, Sep. 2018.
- [3] A. Ashok, M. Govindarasu and V. Ajjrapu, "Online detection of stealthy false data injection attacks in power system state estimation," *IEEE Trans. Smart Grid*, vol. 9, no. 3, pp. 1636-1646, May 2018.
- [4] C. Muscas, P. A. Pegoraro, S. Sulis, M. Pau, F. Ponci and A. Monti, "New Kalman filter approach exploiting frequency knowledge for accurate PMU-based power system state estimation," *IEEE Trans. Instrum. Meas.*, vol. 69, no. 9, pp. 6713-6722, Sep. 2020.
- [5] M. Ahwiadi and W. Wang, "An adaptive particle filter technique for system state estimation and prognosis," *IEEE Trans. Instrum. Meas.*, vol. 69, no. 9, pp. 6756-6765, Sep. 2020.
- [6] A. RezaAbbasi and A. RezaSeifi, "A new coordinated approach to state estimation in integrated power system," *Int. J. Electr. Power Energy Syst.*, vol. 45, no. 1, pp. 152-158, Feb. 2013.
- [7] Y. Liu et al., "Dynamic state estimation for power system control and protection," *IEEE Trans. Power Syst.*, vol. 36, no. 6, pp. 5909-5921, Nov. 2021.
- [8] W. Li, G. Wei, D. Ding, Y. Liu and F. E. Alsaadi, "A new look at boundedness of error covariance of Kalman filtering," *IEEE Trans. Syst., Man, Cybern. A, Syst., Humans*, vol. 48, no. 2, pp. 309-314, Feb. 2018.
- [9] R. Ferrero, P. A. Pegoraro and S. Toscani, "Dynamic synchrophasor estimation by extended Kalman filter," *IEEE Trans. Instrum. Meas.*, vol. 69, no. 7, pp. 4818-4826, Jul. 2020.
- [10] J. Zhao and L. Mili, "Robust unscented Kalman filter for power system dynamic state estimation with unknown noise statistics," *IEEE Trans. Smart Grid*, vol. 10, no. 2, pp. 1215-1224, Mar. 2019.
- [11] C. Wu, M. E. Magaña and E. Cotilla-Sánchez, "Dynamic frequency and amplitude estimation for three-phase unbalanced power system using the unscented Kalman filter," *IEEE Trans. Instrum. Meas.*, vol. 68, no. 9, pp. 3387-3395, Sep. 2019.
- [12] S. Li, Y. Hu, L. Zheng, et al. "Stochastic event-triggered cubature Kalman filter for power system dynamic state estimation," *IEEE Trans. Circuits Syst. II, Exp. Briefs.*, vol. 66, no. 9, pp. 1552-1556, Sep. 2019.
- [13] A. Sharma, S. C. Srivastava and S. Chakrabarti, "A cubature Kalman filter based power system dynamic state estimator," *IEEE Trans. Instrum. Meas.*, vol. 66, no. 8, pp. 2036-2045, Aug. 2017.
- [14] Y. Wang, Y. Sun and V. Dinavahi, "Robust forecasting-aided state estimation for power system against uncertainties," *IEEE Trans. Power Syst.*, vol. 35, no. 1, pp. 691-702, Jan. 2020.
- [15] S. Akhlaghi, N. Zhou and Z. Huang, "A multi-step adaptive interpolation approach to mitigating the impact of nonlinearity on dynamic state estimation," *IEEE Trans. Smart Grid*, vol. 9, no. 4, pp. 3102-3111, Jul. 2018.
- [16] J. Qi, K. Sun, J. Wang and H. Liu, "Dynamic state estimation for multi-machine power system by unscented Kalman filter with enhanced numerical stability," *IEEE Trans. Smart Grid*, vol. 9, no. 2, pp. 1184-1196, Mar. 2018.
- [17] G. Anagnostou and B. C. Pal, "Derivative-free Kalman filtering based approaches to dynamic state estimation for power system with unknown inputs," *IEEE Trans. Power Syst.*, vol. 33, no. 1, pp. 116-130, Jan. 2018.
- [18] Z. Jin, J. Zhao, S. Chakrabarti, L. Ding and V. Terzija, "A hybrid robust forecasting-aided state estimator considering bimodal Gaussian mixture measurement errors," *Int. J. Electr. Power Energy Syst.*, vol. 120, pp. 105962, Sep. 2020.
- [19] J. Zhao and L. Mili, "A framework for robust hybrid state estimation with unknown measurement noise statistics," *IEEE Trans. Ind. Informat.*, vol. 14, no. 5, pp. 1866-1875, May 2018.
- [20] S. Wang, J. Zhao, Z. Huang and R. Diao, "Assessing gaussian assumption of pmu measurement error using field data," *IEEE Trans. Power Del.*, vol. 33, no. 6, pp. 3233-3236, Dec. 2018.
- [21] Y. Sun, Y. Wang, V. Dinavahi, K. Wang and D. Nan, "Robust dynamic state estimation of power system with model uncertainties based on adaptive unscented H $\infty$  filter," *IET Gener. Transm. Dis.*, vol. 13, no. 12, pp. 2455-2463, May 2019.
- [22] J. Zhao, and L. Mili, "Decentralized H-infinity unscented Kalman filter for dynamic state estimation against uncertainties," *IEEE Trans. Smart Grid*, vol. 10, no. 5, pp. 4870-4880, Sep. 2019.
- [23] C. D. Karlgaard, "Nonlinear regression Huber-Kalman filtering and fixed-interval smoothing," *J. Guid. Control Dynam.*, vol. 38, no. 2, pp. 322-330, Feb. 2015.
- [24] B. Chen, Y. Xie, Z. Li, Y. Li and P. Ren, "Asymmetric correntropy for robust adaptive filtering," *IEEE Trans. Circuits Syst. II, Exp. Briefs*, 2021. Doi: 10.1109/TCSII.2021.3122283.
- [25] B. Chen, Y. Xie, X. Wang, Z. Yuan, P. Ren and J. Qin, "Multikernel correntropy for robust learning," *IEEE Trans. Cybern.*, 2021. Doi: 10.1109/TCYB.2021.3110732.
- [26] L. Shi and Y. Lin, "Convex combination of adaptive filters under the maximum correntropy criterion in impulsive interference," *IEEE Signal Process. Lett.*, vol. 21, no. 11, pp. 1385-1388, Nov. 2014.
- [27] T. Ogunfunmi and T. Paul, "The quaternion maximum correntropy algorithm," *IEEE Trans. Circuits Syst. II, Exp. Briefs*, vol. 62, no. 6, pp. 598-602, Jun. 2015.
- [28] J. He, C. Sun, B. Zhang and P. Wang, "Variational Bayesian-based maximum correntropy cubature Kalman filter with both adaptivity and robustness," *IEEE Sens. J.*, vol. 21, no. 2, pp. 1982-1992, Jan. 2021.
- [29] B. Chen, L. Xing, H. Zhao, N. Zheng and J. C. Pri, "Generalized correntropy for robust adaptive filtering," *IEEE Trans. Signal Process.*, vol. 64, no. 13, pp. 3376-3387, Jul. 2016.
- [30] W. Ma, J. Qiu, X. Liu, G. Xiao, J. Duan and B. Chen, "Unscented Kalman filter with generalized correntropy loss for robust power system forecasting-aided state estimation," *IEEE Trans. Ind. Informat.*, vol. 15, no. 11, pp. 6091-6100, Nov. 2019.
- [31] X. Liu, Z. Ren, H. Lyu, Z. Jiang, P. Ren and B. Chen, "Linear and nonlinear regression-based maximum correntropy extended Kalman filtering," *IEEE Trans. Syst., Man, Cybern. A, Syst., Humans*, vol. 51, no. 5, pp. 3093-3102, May 2021.
- [32] S. Fakoorian, A. Santamaria-Navarro, B. Lopez, D. Simon and A. A. Agha-mohammadi, "Towards robust state estimation by boosting the maximum correntropy criterion Kalman filter with adaptive behaviors," *IEEE Robot. Autom. Lett.*, vol. 6, no. 3, pp. 5469-5476, Jul. 2021.
- [33] S. Li, B. Xu, L. Wang and A. A. Razzaqi, "Improved maximum correntropy cubature Kalman filter for cooperative localization," *IEEE Sens. J.*, vol. 20, no. 22, pp. 13585-13595, Nov. 2020.
- [34] M. V. Kulikova, "Chandrasekhar-based maximum correntropy Kalman filtering with the adaptive kernel size selection," *IEEE Trans. Autom. Control*, vol. 65, no. 2, pp. 741-748, Feb. 2020.
- [35] M. Guo, C. Guo and C. Zhang, "A framework of cubature - H $_2$ / H $\infty$ -fault detection and robust H-infinity Kalman filter of ship SINS/GNSS integrated system," *IEEE Access*, vol. 8, pp. 196963-196974, 2020.
- [36] Z. Huang, P. Du, D. Kosterev and S. Yang, "Generator dynamic model validation and parameter calibration using phasor measurements at the point of connection," *IEEE Trans. Power Syst.*, vol. 28, no. 2, pp. 1939-1949, May 2013.



**Yaoqiang Wang** (Senior Member, IEEE) received his B.S. degree from Hangzhou Dianzi University, Hangzhou, China, in 2006; and his M.S. and Ph.D. degrees from the Harbin Institute of Technology, Harbin, China, in 2008 and 2013, respectively.

He is currently working with the School of Electrical Engineering, Zhengzhou University, Zhengzhou, China. He is also serving as the Director of the Henan Provincial Engineering Research Center of Power Electronics and Energy Systems (HERC-PEES). He has authored or coauthored more than 60 technical papers including over 50 journal papers, and is the holder of more than 20 patents. His current research interests include power electronics, renewable power generation, flexible power distribution, electric motor drive, and electrified transportation.



**Zhiwei Yang** (Student Member, IEEE) received his B.S. degree in Electric Power System & its Automation from Henan University of Technology, Zhengzhou, China, in 2019. He is currently pursuing the M.S. degree in Electrical Engineering at Zhengzhou University, Zhengzhou, China. His research interests include theoretical and

algorithmic studies in power system estimation.



**Yi Wang** (Member, IEEE) received his B.S. degree from Luoyang Institute of Science and Technology, Luoyang, China, in 2014; and received his Ph.D. degree from Hohai University, Nanjing, China, in 2020.

He was a visiting scholar at the University of Alberta between 2018 and 2019. His current research interests include theoretical and algorithmic studies in power system estimation, parameters identification, power system dynamics, signal processing, and cyber security. He is also an active reviewer for many international journals.



**Venkata Dinavahi** (Fellow, IEEE) received the B.Eng. degree in electrical engineering from Visvesvaraya National Institute of Technology (VNIT), Nagpur, India, in 1993, the M.Tech. degree in electrical engineering from the Indian Institute of Technology (IIT) Kanpur, India, in 1996, and the Ph.D.

degree in electrical and computer engineering from the University of Toronto, Ontario, Canada, in 2000.

He is currently a Professor with the Department of Electrical and Computer Engineering, University of Alberta, Edmonton, Alberta, Canada. He is a Fellow of the Engineering Institute of Canada. His research interests include real-time simulation of power systems and power electronic systems, electromagnetic transients, device level modeling, large-scale systems, and parallel and distributed computing.



**Kewen Wang** (Member, IEEE) received his B.S. degree from the Zhengzhou Institute of Technology, Zhengzhou, China, in 1985; his M.S. degree from Tianjin University, Tianjin, China, in 1988; and his Ph.D. degree from Hong Kong Polytechnic University, Hong Kong, China, in 2000.

He is currently a Professor with the School of Electrical Engineering, Zhengzhou University, Zhengzhou, China. His research interests include power electronics, renewable power generation, power system stability analysis and control, reactive power optimization.



**Jun Liang** (Senior Member, IEEE) received his B.S. degree in Electric Power System & its Automation from the Huazhong University of Science and Technology, Wuhan, China, in 1992; and his M.S. and Ph.D. degrees in Electric Power System & its Automation from the China Electric Power Research Institute (CEPRI), Beijing, in 1995 and 1998, respectively.

From 1998 to 2001, he was a Senior Engineer with CEPRI. From 2001 to 2005, he was a Research Associate with Imperial College London, U.K. From 2005 to 2007, he was with the University of Glamorgan as a Senior Lecturer. He is currently a Professor in Power Electronics with the School of Engineering, Cardiff University, Cardiff, U.K. He is the Coordinator and Scientist-in-Charge of two European Commission Marie-Curie Action ITN/ETN projects: MEDOW (€3.9M) and InnoDC (€3.9M). His research interests include HVDC, MVDC, FACTS, power system stability control, power electronics, and renewable power generation.

Prof. Liang is a Fellow of the Institution of Engineering and Technology (IET). He is the Chair of IEEE UK and Ireland Power Electronics Chapter. He is an Editorial Board Member of CSEE JPES. He is an Editor of the IEEE Transactions on Sustainable Energy.